The effects of 3-D anelasticity (Q) structure on surface wave phase delays

Youyi Ruan and Ying Zhou

Department of Geosciences, Virginia Polytechnic Institute and State University, Blacksburg, VA 24061, *USA. E-mail: chukren@vt.edu*

SUMMARY

Lateral variations in anelasticity (Q) provide important constraints complementary to 3-D wave speed variations in mapping 3-D thermal and compositional structures in the mantle. In present-day joint tomographic inversions of global velocity and anelasticity (Q) structure, 3-D anelastic dispersion effects on surface waves have been ignored. In this work, we quantify the effects of 3-D Q structure on surface wave phase delays by simulating wave propagation in 3-D wave speed and 3-D Q models using a spectral element method (SEM). We compare phase delays caused by 3-D Q structure and those caused by 3-D velocity structure. Our results show that (1) roughly 15–20 per cent of the observed phase delays (traveltimes) in long-period surface waves are due to 3-D Q structure; this implies that neglecting 3-D anelastic dispersion effects can lead to biased velocity models in seismic tomography; (2) the effects of Q perturbations on surface wave phase delays are frequency dependent as a result of local S-wave anelastic dispersion, frequency-dependent depth sensitivity of surface waves as well as the 3-D distribution of Q anomalies. In our numerical experiments, the significance of 3-D anelastic dispersion increases with wave period, and the frequency dependence is most apparent in the period range between 60 and 150 s and becomes weaker at 150–200 s and (3) assuming a thermal origin, anelastic delays caused by 'hot' anomalies (or advances caused by 'cold' anomalies) are correlated with elastic delays (or advances), but their relation is not linear: the ratio between anelastic and elastic delays (or advances) becomes larger for 'hotter' anomalies than for 'colder' anomalies.

Key words: Elasticity and anelasticity; Surface waves and free oscillations; Seismic attenuation; Seismic tomography.

GJI Seismology

1 INTRODUCTION

In the past decades, lateral variations in seismic wave speeds in the mantle have been mapped out at a global scale by seismic tomographic studies (e.g. Grand 1987; Su *et al.* 1994; Master *et al.* 1996; Ritsema & Van Heijst 2000; Zhou *et al.* 2006). It is known that using only wave speed structure in the upper mantle is not possible to distinguish between thermal and chemical origins of mantle heterogeneities. The anelasticity (Q) structure of the Earth's mantle is very sensitive to temperature perturbations, therefore lateral variations in Q can be applied as a valuable constraint complementary to 3-D wave speed structure to understand the thermal and chemical variations as well as the dynamics of the Earth's interior.

The effects of anelasticity on the Earth's free oscillations as well as on propagating surface waves and body waves have been documented in the 1970s (e.g. Liu *et al.* 1976; Kanamori & Anderson 1977). Several 1-D (radial) Q models have been developed (e.g. Dziewonski & Anderson 1981) and widely used in today's seismological studies. However, compared to 3-D wave speed tomography, studies of 3-D anelasticity (Q) structure in the mantle

have been lagging behind. In the past two decades, efforts have been made to image the 3-D anelasticity structure in the mantle using both surface waves (e.g. Romanowicz 1995; Selby & Woodhouse 2002; Gung & Romanowicz 2004; Dalton *et al.* 2008) and body waves (e.g. Reid *et al.* 2001; Warren & Shearer 2002). In the upper mantle, lateral variations in Q differ considerably among those models (e.g. Dalton *et al.* 2008). These discrepancies are partly due to the fact that seismic amplitudes can be affected by both 3-D anelastic structure as well as 3-D elastic wave speed structure through wave focusing and defocusing. It is difficult to separate the two contributing effects and different research groups often take different approaches in handling the focusing and defocusing effects in tomographic practices (e.g. Selby & Woodhouse 2000; Dalton *et al.* 2008). The importance of a joint inversion of 3-D velocity and Q using both amplitude and phase delay measurements has been appreciated in several recent surface wave studies (e.g. Billien *et al.* 2000; Dalton *et al.* 2008), however, the effects of 3-D Q structure on surface wave phase delays have so far received little attention. The focus of this paper is to quantify the effects of 3-D anelastic structures on surface wave phase delays, in particular, how do

phase delays caused by 3-D Q structure compared with phase delays caused by 3-D wave speed structure.

It is known that lateral compositional heterogeneities in the mantle have only secondary effects on seismic wave speed and anelasticity (e.g. Faul & Jackson 2005). In this study, we construct our 3-D Q models using a 3-D wave speed model S20RTS of Ritsema & Van Heijst (2000), assuming that both velocity and Q perturbations are due to temperature variations. We simulate wave propagation in 3-D global models using the Spectral Element Method (Komatitsch & Tromp 1999, 2002), and we measure phase delays between fundamental-mode surface waves generated in earth models with and without the presence of 3-D Q structures. The same wave propagation experiments are done for earth models with and without 3-D wave speed structures to measure phase delays caused by 3-D wave speed structure. Comparisons between phase delays caused by 3-D wave speed and 3-D Q structure show that roughly 15–20 per cent of the observed phase delays (traveltimes) in long-period surface waves are due to 3-D anelasticity (Q) structure. This result agrees with estimates made based upon 3-D sensitivity kernels (Zhou 2009). We show that 3-D anelastic effects are dependent upon mineralogical parameters applied in generating global Q models. We investigate 3-D anelastic dispersion effects in continental and oceanic paths and the non-linear relation between delay times caused by 'elastic' and 'anelastic' mechanisms.

2 QUALITY FACTOR Q AND ANELASTIC DISPERSION

The effects of the anelasticity of Earth material on seismic waves can be accounted for by considering the relaxation of elastic moduli. The relaxation of elastic moduli is associated with energy dissipation (internal friction) of seismic waves and can be characterized by the quality factor Q – energy loss per cycle. It is known that anelasticity affects seismic waves in two aspects: amplitude attenuation and anelastic dispersion; and the latter describes variations of wave speed with frequency. These effects can be accounted for by using complex and frequency dependent moduli (Dahlen & Tromp 1998):

$$\mu \rightarrow \mu_0 \left[1 + \frac{2}{\pi} Q_\mu^{-1} \ln\left(\frac{\omega}{\omega_0}\right) + i Q_\mu^{-1} \right], \tag{1}$$

$$\kappa \rightarrow \kappa_0 \left[1 + \frac{2}{\pi} Q_\kappa^{-1} \ln\left(\frac{\omega}{\omega_0}\right) + i Q_\kappa^{-1} \right], \tag{2}$$

where μ_0 and κ_0 are the shear and bulk moduli at a reference frequency ω_0, and Q_μ and Q_κ are the corresponding quality factors. The imaginary part of the modulus in eqs (1) and (2) represents amplitude attenuation, and the frequency-dependent real part describes velocity dispersion. In this study, we focus on seismic wave propagation speeds in the presence of 3-D Q structure. The effects of anelasticity on surface wave amplitudes will be discussed in a separate paper. To the first order, the real part of the complex moduli in eqs (1) and (2) leads to dispersion of wave speed $V(\omega)$ and can be written as (Dahlen & Tromp 1998)

$$V(\omega) = V(\omega_0) \left[1 + \frac{1}{\pi Q} \ln\left(\frac{\omega}{\omega_0}\right) \right], \tag{3}$$

where $V(\omega_0)$ is the wave speed at a reference frequency ω_0, and Q is the quality factor.

The relaxation of stresses and strains in wave propagation is a result of irreversible changes of crystal defect structures and grain boundaries of Earth material. Assuming thermally activated processes, the quality factor Q is dependent upon rheology parameters of the material, mantle temperature and pressure as well as the frequency of the wave (e.g. Jackson & Anderson 1970; Karato & Spetzler 1990),

$$Q(\omega, T) = A \omega^\alpha \exp\left[\frac{\alpha(E^* + PV^*)}{RT} \right], \tag{4}$$

where E^* and V^* are the activation energy and activation volume of anelastic relaxation, respectively. These rheology parameters can be measured in experimental studies for upper mantle material (e.g. olivine), and they vary in a relatively wide range (e.g. Béjina *et al.* 2003). Under upper mantle condition, the activation energy E^* of olivine varies from 300 to 500 KJ mol^{-1}, and the activation volume V^* ranges from 5 to 30 cm^3 mol^{-1} (Jackson *et al.* 2002). A is a constant associated with properties of the material such as the grain size (Jackson *et al.* 2002; Faul & Jackson 2005) and R is the gas constant. From both mineral physics experiments and seismological observations, Q exhibits only weak dependence upon frequency and the coefficient α is roughly between 0.1 and 0.4 and it does not vary significantly with temperature (e.g. Anderson & Minster 1979; Smith & Dahlen 1981; Karato & Spetzler 1990; Jackson & Paterson 1993; Jackson 2000; Shito *et al.* 2004). In surface wave studies, resolving the frequency dependence of Q is still a challenging task and a constant Q absorption-band model (e.g. Liu *et al.* 1976; Kanamori & Anderson 1977) has been widely used in wave propagation simulations as well as in inversions of velocity and Q structures (e.g. Dziewonski & Anderson 1981; Komatitsch & Tromp 1999; Dalton *et al.* 2008). In this study, we neglect the weak frequency dependence of Q in wave propagating experiment and the temperature and pressure dependence of Q can be rewritten as

$$Q(\omega, T) = A \exp\left[\frac{\alpha(E^* + PV^*)}{RT} \right]. \tag{5}$$

3 WAVE PROPAGATION IN 3-D Q AND 3-D VELOCITY MODELS

The focus of this paper is to simulate wave propagation in 3-D wave speed earth models and 3-D Q models and compare the effects of 3-D wave speed variations and the effects of 3-D Q perturbations on surface wave phase delays. In this study, we construct our 3-D tomographic-like Q model using a 3-D wave speed model S20RTS of Ritsema & Van Heijst (2000), assuming that both velocity and Q perturbations are due to temperature variations.

3.1 1-D reference Q model

Model S20RTS describes *S*-wave velocity perturbations in the mantle with respect to the Preliminary Reference Earth Model (PREM) (Dziewonski & Anderson 1981). A radial Q structure has been incorporated in the model. In this study, we assume a thermally activated Q mechanism and construct self-consistent reference radial (1-D) Q profile and lateral (3-D) variations using eq. (5). In constructing the reference radial (1-D) Q model, we use a reference geotherm in the upper mantle assuming a half-space cooling mantle,

$$T(z) = T_s + (T_m - T_s) \text{erf}\left(\frac{z}{2\sqrt{\kappa \tau_c}} \right), \tag{6}$$

where the surface temperature T_s is assumed to be $0\,°C$ and the mantle temperature T_m is assumed to be $1300\,°C$. We use a thermal diffusivity κ of $1 \times 10^{-6}\,\text{m}^2\,\text{s}^{-1}$ and a cooling age τ_c of 60 Myr.
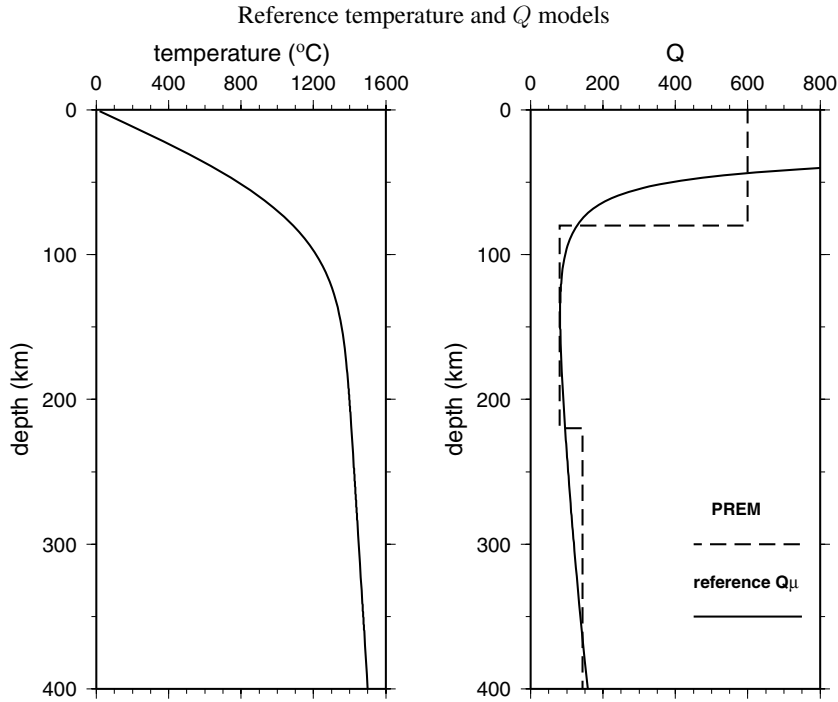
Reference temperature and Q models

Figure 1. (a) Reference geotherm assuming a half-space cooling model with mantle temperature $T_M = 1300\,^{\circ}\text{C}$ and cooling age $\tau_c = 60$ Myr. An adiabatic thermal gradient $0.5\,^{\circ}\text{C}\,\text{km}^{-1}$ has been added throughout the mantle. Only the uppermost 400 km of the profile is plotted. (b) Reference Q model (Q_μ) derived using the temperature model and mineralogy parameters $E^* = 470\,\text{KJ}\,\text{mol}^{-1}$ and $V^* = 17\,\text{cm}^3\,\text{mol}^{-1}$. PREM Q_μ profile is plotted in dashed line for reference.

An adiabatic thermal gradient of $0.5\,^{\circ}\text{C}\,\text{km}^{-1}$ is added throughout the mantle. The reference mantle temperature profile is plotted in Fig. 1. It is noteworthy that these geothermal parameters are not well constrained, and parameters are chosen based on current estimates to produce a reasonable globally averaged geotherm in the upper mantle (e.g. Shapiro & Ritzwoller 2004; Faul & Jackson 2005).

Based upon the 1-D background temperature model, we calculate a reference 1-D Q model using eq. (5) with the following rheology parameters: activation energy $E^* = 470\,\text{KJ}\,\text{mol}^{-1}$, activation volume $V^* = 17\,\text{cm}^3\,\text{mol}^{-1}$ and α value of 0.1. We use the radial pressure profile in model PREM in constructing our reference radial Q structure, and choose a constant $A = 1.394$ such that our 1-D reference Q model is close to PREM. In Fig. 1, we plot our reference Q model together with the 1-D Q structure in PREM in the top 400 km. In the uppermost 80 km, PREM has a constant Q value of 600, while Q values in our reference model decrease from over 1000 to 150 due to the exponential temperature dependence. Considering that the lithosphere is cold and mostly elastic, and anelasticity is related to $1/Q$ rather than Q, it is safe to use high Q values in the lithosphere. Even though it is reasonable to assume a mostly elastic lithosphere, especially in the top 50 km, we discuss the effects of low Q values in the lithosphere in Section 4. At the depth range of 80–220 km, Q values in our model are very close to PREM, except for that there are two sharp discontinuities at depths of 80 km and 220 km in model PREM. Between 220 and 300 km, our 1-D Q model shows slightly lower Q values than PREM. Overall, our reference 1-D Q model constructed using eq. (5) is very close to PREM Q model.

3.2 3-D Q models

In this study, we construct a 3-D tomographic-like Q model using a 3-D wave speed model S20RTS. Assuming thermally activated

processes of velocity and Q perturbations, wave speed is dependent upon both temperature and wave frequency (Kanamori & Anderson 1977; Karato 1993),

$$V(\omega, T) = V_0(T)\left[1 + \frac{1}{Q\pi}\frac{E^* + PV^*}{RT} + \frac{1}{Q\pi}\ln\omega\tau_0\right], \quad (7)$$

where τ_0 is a constant in the order of 10^{-12} to 10^{-13} s, approximately the period of the fundamental thermal vibrations for atomic relaxation (Jackson & Anderson 1970), and V_0 is the 'anharmonic' elastic velocity which corresponds to the seismic velocity at $Q = \infty$. Taking derivative of eq. (7), to the first order, temperature perturbations can be calculated from velocity perturbations using the temperature partial derivative $\partial\ln V/\partial T$ (Karato 1993),

$$\frac{\partial\ln V}{\partial T} = \frac{\partial\ln V_0}{\partial T} - \frac{1}{Q\pi}\frac{E^* + PV^*}{RT^2}. \quad (8)$$

Note that to the first order, the frequency-dependent term (anelastic dispersion) in eq. (7) does not contribute to the temperature partial derivative. The partial derivative $\partial\ln V_0/\partial T \approx -0.76 \times 10^{-4}\,\text{K}^{-1}$ for S waves (Isaak 1992), and it is insensitive to crystal structures (Duffy & Anderson 1989). Taking temperature derivative of equation (5), fractional perturbations in Q can be calculated from perturbations in temperature T by

$$\frac{\delta Q}{Q} = -\alpha\frac{E^* + PV^*}{RT^2}\delta T. \quad (9)$$

Like many other global velocity models, model S20RTS describes 3-D wave speed variations in the mantle but has assumed a radial structure of Q (PREM Q structure). This is not self consistent in the sense that lateral variations in temperature should give rise to lateral variations in both velocity and Q. In this study, we compute its corresponding 3-D Q structure using eqs (8) and (9) using an iterative approach: (1) calculate 3-D temperature perturbations δT

from the 3-D velocity perturbations in S20RTS using the temperature partial derivative $\partial \ln V_S / \partial T$ assuming a 1-D initial temperature and Q structure as described in Section 3.1, (2) update the local temperature with perturbations obtained from step (1) and calculate the corresponding perturbations in Q using eq. (9), (3) update $\partial \ln V_S / \partial T$ in eq. (8) using the new temperature and Q values and go back to step (1), iterate until perturbations in temperature and Q converge.

Maps of the 3-D velocity model (S20RTS) and the corresponding 3-D Q model, **Q3DM**$_M$, at 100 km depth are shown in Fig. 2. The fractional perturbations in $1/Q$ are with respect to our 1-D reference Q model. The resulting 3-D Q model is highly correlated with the 3-D velocity model: mid-ocean ridges are characterized by slow anomalies and lower-than-average Q values, stable continental interiors show fast anomalies and higher-than-average Q values. Compared with recent tomographic 3-D Q models (e.g. Dalton *et al.* 2008), the strength (rms) of Q perturbations in our 3-D model is comparable to those tomographic studies. For example, perturbations in $1/Q$ at a depth of 100 km are in the range of -0.01 to 0.011 in our model, comparable to -0.0125 to 0.01 in the model of Dalton *et al.* (2008); the corresponding fractional perturbations are in the range of -99.9 to 107.5 per cent in our model, comparable to -100 to 80 per cent in their model. 2-D Love-wave as well as Rayleigh wave Q maps are plotted in Fig. 3, which are also comparable to recent 2-D surface wave Q models (e.g. Dalton & Ekström 2006).

It is important to point out that we have considered the Q dependence of temperature partial derivative $\partial \ln V / \partial T$ in constructing 3-D temperature and Q variations from 3-D velocity variations. The resulting 3-D earth model are self-consistent in that both Q and velocity are results of 3-D variations in mantle temperature.

3.3 Wave propagation in 3-D earth models and phase delay measurements

The effects of lateral thermal anomalies in seismic observables can be modelled by simulating wave propagation in earth models with 3-D velocity (S20RTS) and 3-D Q structures. In this study, we investigate the effects of 3-D wave speed structure and the effects of 3-D anelastic dispersion separately, and compare long-period surface wave phase delays caused by 3-D Q structure through 3-D anelastic dispersion with phase delays caused by 3-D elastic wave speed structure. We simulate wave propagation in 3-D velocity and 3-D Q models using the Spectral Element Method (SEM) (Komatitsch & Tromp 1999). The SEM incorporated anelasticity in wave propagation using three standard linear solids assuming Q is independent of frequency (absorption-band model). Twelve earthquake events and 801 seismic stations around the world were chosen for our numerical experiments to provide good path coverage.

We simulate wave propagation in four different Earth models (see Table 1) for each event. In the case of examining the effects of 3-D wave speed structure ('3-D elastic effects' hereinafter) on
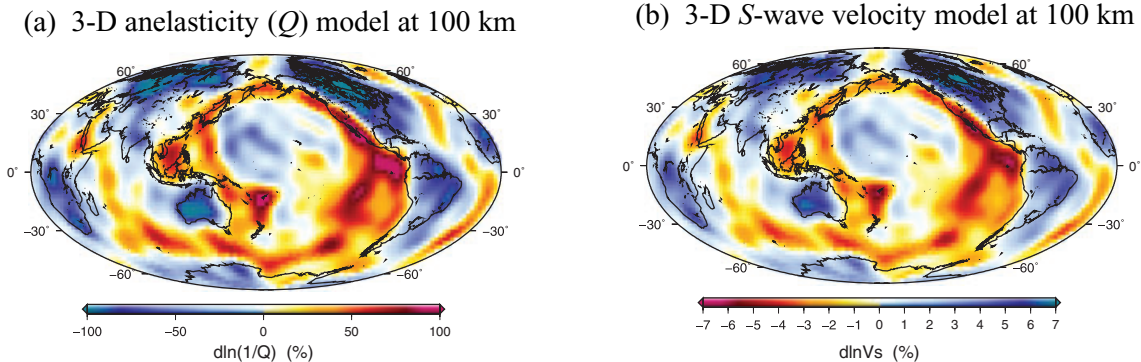
(a) 3-D anelasticity (Q) model at 100 km

(b) 3-D S-wave velocity model at 100 km

Figure 2. (a) 3-D anelasticity model at a depth of 100 km. Fractional perturbations in $1/Q$ are in the range of -99.9 to 107.5 per cent, comparable to recent tomographic models (e.g. Dalton *et al.* 2008). (b) 3-D shear wave velocity model S20RTS (Ritsema & Van Heijst 2000) at a depth of 100 km. The 3-D Q model and the 3-D velocity model are correlated as we assume both of them are originated from temperature variations.
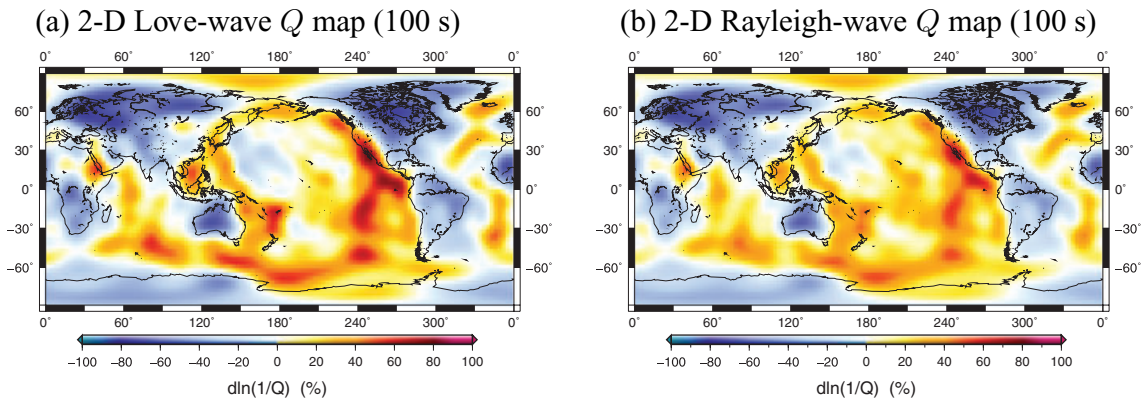
(a) 2-D Love-wave Q map (100 s)

(b) 2-D Rayleigh-wave Q map (100 s)

Figure 3. 2-D surface wave Q maps calculated for our 3-D anelastic earth model. (a) 2-D Love-wave Q map at 100 s for our 3-D anelastic earth model (S20RTS + 3D Q), fractional variations in $1/Q$ are with respect to Love-wave Q in the earth model with 1-D reference Q structure (S20RTS + 1D Q). Fractional variations in Love-wave $1/Q$ are in the range of -78.2 to 85.4 per cent. (b) The same as (a) but for 100-s Rayleigh waves, and the fractional variations are between -74.6 and 72.6 per cent.

Table 1. Models for 3-D wave propagation.

Models	Model no.	Velocity	Anelasticity (Q)
Elastic delay measurement	I	1-D (PREM)	1-D (PREM)
	II	3-D (S20RTS)	1-D (PREM)
Anelastic delay measurement	III	3-D (S20RTS)	1-D (**Q1DM$_M$**)
	IV	3-D (S20RTS)	3-D (**Q3DM$_M$**)

surface wave phase delays, we measure phase differences between synthetic seismograms generated in model (I)—1-D velocity and 1-D Q and model (II)—3-D velocity and 1-D Q. The Q structures in model (I) and (II) are identical, therefore, differences in surface wave traveltimes are due to the 3-D velocity structures (elastic delay = $t_{3-DV} - t_{1-DV}$). The 1-D velocity and 1-D Q models used in this case are from PREM (Fig. 1) and the 3-D velocity model is S20RTS. In the case of examining the effects of 3-D anelastic dispersion (3-D Q effects), we measure phase differences between seismograms generated in model (III)—3-D velocity and 1-D Q and model (IV)—3-D velocity and 3-D Q. In this case velocity structures are the same in the two models, and differences in surface wave traveltimes are due to 3-D anelastic perturbations (anelastic delay = $t_{3-DQ} - t_{1-DQ}$). The 1-D Q and 3-D Q models have been described in Sections 3.1 and 3.2, and perturbations in the 3-D Q models are comparable to recent tomographic Q models (e.g. Dalton *et al.* 2008).

Surface wave phase delays are measured using a multitaper technique (Laske & Masters 1996; Zhou *et al.* 2004). The tapers used in this paper are five 2.5-π prolate spheroidal eigentapers (Slepian 1978) with narrowly concentrated spectra. Measurements made with this technique show reduced bias in spectral estimates in surface wave studies (Laske & Masters 1996). Phase delays and associated errors are estimated by least-square fitting of measurements made with these five orthogonal tapers. We measure fundamental-mode surface wave phase delays at frequencies (periods) from 5 mHz (200 s) to 20 mHz (50 s). Fundamental-mode surface waves, especially Love waves, can be contaminated by higher-mode surface waves at short epicentral distances. We carefully choose measurement windows that contain mostly fundamental-mode surface wave energy to minimize contamination of higher-mode surface waves. Because of the dispersion of surface waves, we filter seismograms at two frequency bands, 50–100 s and 100–200 s, and choose measurement windows correspondingly. We examine every single measurement and correct/remove measurements with cycle

skip problems, this left ~7600 minor-arc Love waves and ~8500 Rayleigh waves for this study.

For some event-station pairs, seismic waves travel along continent–ocean boundaries where strong velocity contrast can be expected. Surface waves along these paths sometimes show two separate arrivals, one travels in the continental side where seismic velocity is higher than the reference velocity and the other one travels in the oceanic side where seismic velocity is relatively lower. An example of seismogram with apparent multipathing signals is plotted in Fig. 4. In this study, we choose to exclude those paths from our measurements.

Examples of synthetic seismograms from numerical simulations are shown in Fig. 5. The transverse and vertical component seismograms at station ANMO have been bandpass filtered between 6.7 and 20 mHz. The top two traces in (a) and (b) show differences in seismograms caused by 3-D Q structure, and the bottom two traces show differences of surface waves caused by 3-D velocity structure. Frequency-dependent delay-time measurements are plotted in Fig. 5(d) for this example path. At a period of 100 s, the 3-D velocity variations delay the arrival time of the fundamental-mode Love wave by ~65 s and Rayleigh wave by ~73 s for this particular path; delay times caused by 3-D anelastic dispersion are ~14 s for the Love wave and ~21 s for the Rayleigh wave. The 3-D anelastic dispersion effects (difference between 3-D Q and 1-D Q models) on phase delays are about 1/4 of the phase delays caused by 3-D velocity structure (differences between 3-D velocity and 1-D velocity models). More detailed analysis on the anelastic dispersion effects will be be discussed in detail in Section 4. It is also noteworthy that amplitudes variations in this example show that the effects of 3-D velocity structure on surface wave amplitudes (focusing/defocusing) are more prominent than the effects of 3-D Q structure, this is consistent with estimates made based upon 3-D sensitivity kernels (Zhou 2009) and amplitude measurements will be discussed in a separate paper.
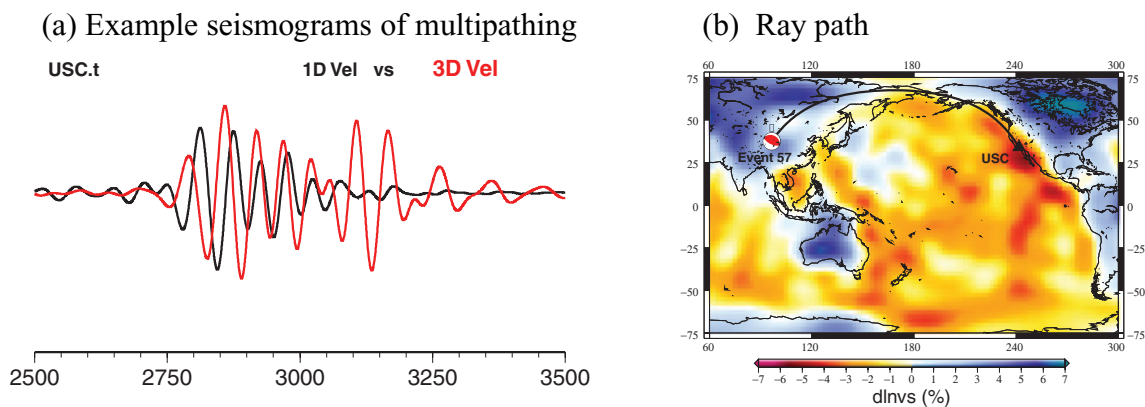

Figure 4. (a) Example multipathing seismograms. The seismograms are transverse-component synthetic seismograms at station USC for a ray path shown in (b). In this example, surface waves in the 3-D velocity model (red trace) show an additional late arrival compared to the seismogram in 1-D velocity model (black trace). (b) Reference ray path along which multipathing arrivals are observed.
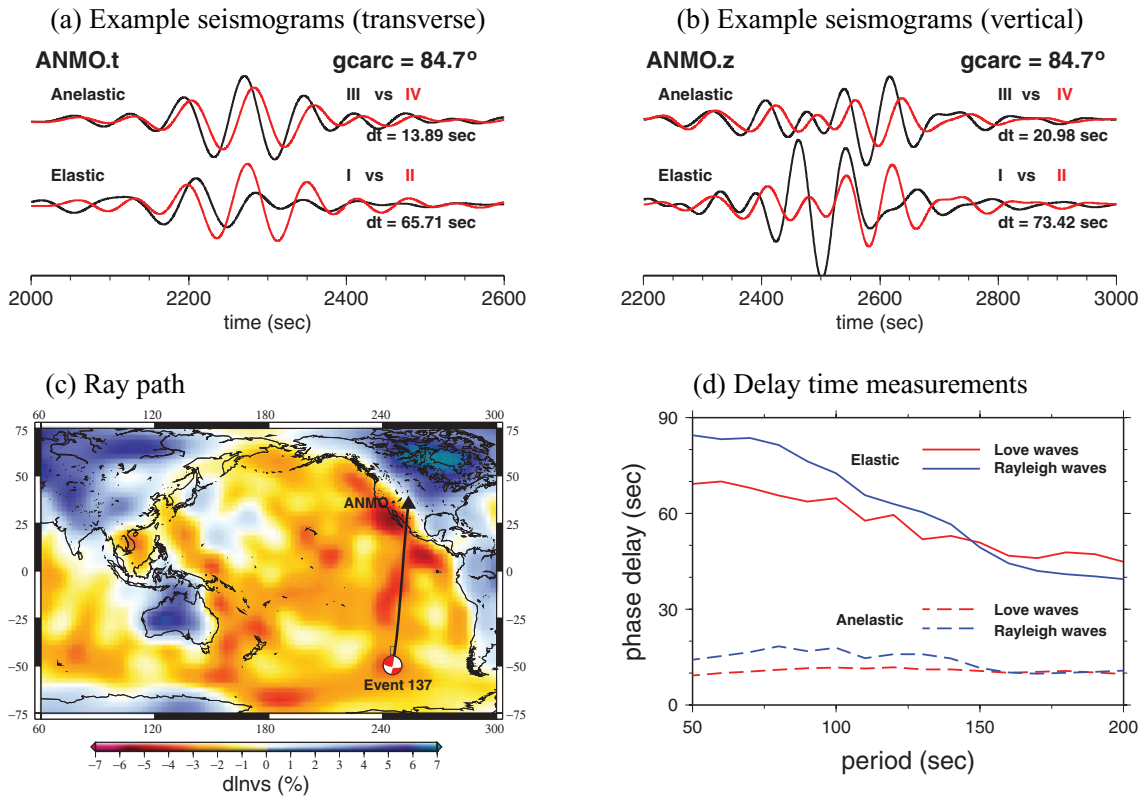
Figure 5. Example transverse (a) and vertical (b) synthetic seismograms at station ANMO, bandpass filtered between 6.7 and 20 mHz. Top seismogram pairs show effects due to anelastic perturbations, black seismograms are generated using model (III)—3-D velocity and 1-D Q, red seismograms are generated using model (IV)—3-D velocity and 3-D Q. Bottom seismogram pairs show differences due to elastic perturbations: black traces are generated using model (I)—1-D velocity and 1-D Q; red traces are generated using model (II)—3-D velocity and 1-D Q. Delay times measured at 100 s using multitaper technique are indicated below the traces. The ray path of the seismograms is shown in (c) and measured elastic and anelastic delay times as a function of period are plotted in (d).

4 3-D ANELASTIC EFFECTS ON SURFACE WAVES AND FREQUENCY DEPENDENCE

In Fig. 6, we compare Love-wave phase delays caused by 3-D velocity structure with those caused by 3-D Q structure. Each dot in the scatterplot represents two phase delay measurements made for the same source–receiver pair; the horizontal axis is the elastic delay $t_{3-DV} - t_{1-DV}$ and the vertical axis is the anelastic delay $t_{3-DQ} - t_{1-DQ}$. Measurement errors estimated using the multitaper technique are indicated by black crosses. There are approximately 6000 measurements in each scatterplot at periods of 60, 100 and 200 s. As expected, the elastic delays and anelastic delays are highly correlated as the velocity and Q structures are correlated.

The anelastic effects on surface wave phase delays are frequency dependent. This is due to local S-wave anelastic dispersion, frequency-dependent depth sensitivity of surface waves as well as the 3-D distribution of Q anomalies. Generally speaking, anelastic delays become more significant in long-period surface waves than in short-period surface waves. For Love waves at 60 s, the ratio between anelastic delays and elastic delays is roughly 0.17. For 100- and 200-s Love waves, the ratio of anelastic delays to elastic delays increases to 0.22 and 0.27, respectively. The depth sensitivity kernels of fundamental-mode surface waves calculated for model PREM at corresponding periods are plotted next to each scatterplot for reference. The rms values of the 3-D anelasticity model and 3-D velocity model as function of depth are also plotted. The depth

sensitivity functions show that short-period Love waves are sensitive to shallow structures where Q values are relatively high and variations of $1/Q$ are relatively weak. Therefore, weaker anelastic effects on surface waves are expected. Long-period Love waves are more sensitive to deeper structures in our 3-D Q model, and Q variations are large in the low Q zone at depth of 80–200 km. Therefore, the contribution of anelastic dispersion to long-period surface wave phase delays becomes more prominent.

Comparisons between anelastic delays and elastic delays for Rayleigh waves are shown in Fig. 7. The ratios of anelastic delays to elastic delays also show strong frequency dependence. For 60-s Rayleigh waves, this ratio is approximately 0.21, and for 100- and 200-s Rayleigh waves, the ratio increases to roughly 0.24 and 0.27. This frequency dependence can be explained by the depth sensitivity of Rayleigh waves and the rms of the models. In the uppermost 100 km, the ratio between the rms of the 3-D velocity model and the rms of the 3-D Q model is large. Therefore, for short-period Rayleigh waves, which are more sensitive to shallow structure, anelastic dispersions are relatively weak compared with elastic delays. At depths below 100 km, the ratio between the rms of the 3-D velocity model and the rms of the 3-D Q model becomes smaller. Therefore, Rayleigh waves at 100 and 200 s, which are more sensitive to structures in this depth range, show stronger anelastic dispersion than short-period waves. In general, Rayleigh waves are less sensitive to shallow structures than Love waves, and they are more sensitive to structures in depth range of 80–300 km (the low Q zone in our model), therefore, 3-D anelastic dispersion effects are more prominent in Rayleigh waves than Love waves.
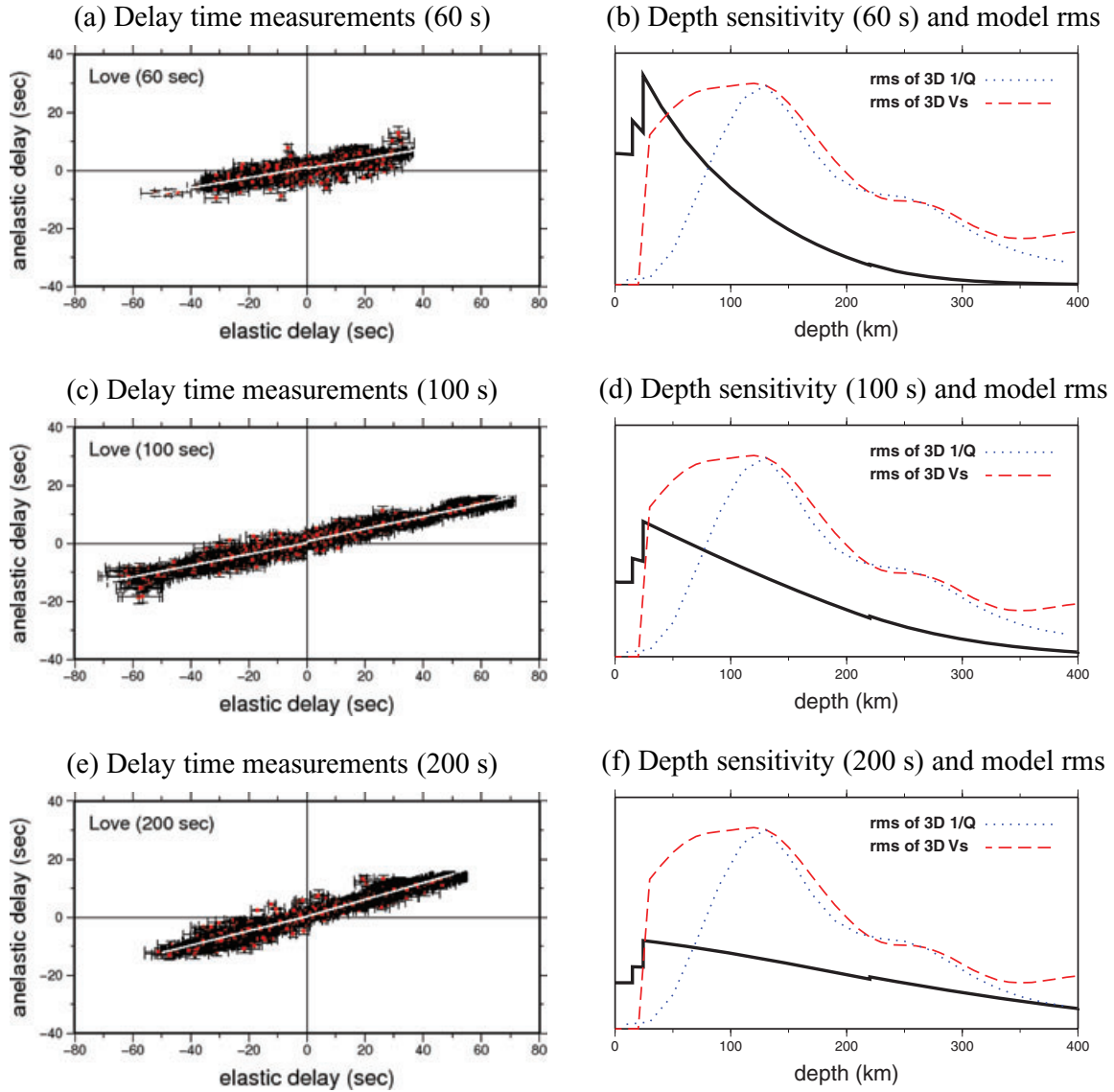
Anelastic effects on Love-wave phase delays

(a) Delay time measurements (60 s)

(b) Depth sensitivity (60 s) and model rms

(c) Delay time measurements (100 s)

(d) Depth sensitivity (100 s) and model rms

(e) Delay time measurements (200 s)

(f) Depth sensitivity (200 s) and model rms

Figure 6. Comparison of elastic delays and anelastic delays on Love waves at periods of (a) 60 s, (c) 100 s and (e) 200 s. In the scatterplots, the horizontal coordinate of the scatterplots is elastic phase delay ($t_{3-DV} - t_{1-DV}$) and the vertical coordinate is anelastic phase delay ($t_{3-DQ} - t_{1-DQ}$). Errors estimated using the multitaper technique are indicated by black crosses. Least-square-fitted slope of each scatterplot (white line) shows the ratio between anelastic and elastic effects. These ratios are 0.17 at 60 s, 0.22 at 100 s and 0.27 at 200 s, showing a strong frequency dependence of anelastic effects. Radial sensitivity ($\partial c/\partial \beta$) of fundamental-mode Love waves at corresponding period and rms of 3-D Q ($\delta \ln (1/Q)$) and 3-D velocity ($\delta \ln V_S$) models are plotted in (b), (d) and (f) as functions of depth. Sensitivity of long-period Love waves show that they are more sensitive to the low Q zone (80–300 km) than short-period Love waves, therefore stronger anelastic dispersion effects are expected at longer periods.

Based upon the comparisons, we can estimate the fractional contribution of anelastic dispersion to the total surface wave phase delays. At 100 s, the slope of scatterplot is roughly 0.22 for Love waves and 0.24 for Rayleigh waves, this indicates that assuming a thermal origin of mantle anomalies, phase delays caused by 3-D Q structure accounts for roughly 17–19 per cent of the total observed delay times. At 200 s, anelastic dispersion effects account for approximately 21 per cent of the total delay times for both Love waves and Rayleigh waves. At 60 s, the percentage decreases to around 15–17 per cent. However, it is important to note that short-period surface waves, especially Love waves, are sensitive to shallow lithosphere structure, and anelastic dispersion of short-period surface

waves depends upon Q structures at shallow depths. Because of the exponential temperature dependence, Q values in our reference models are much larger than PREM in the uppermost 50 km. Recent studies (e.g. Durek & Ekström 1996) suggested a Q value of 300 in the lithosphere. A decrease in background Q will result in an increase in the sensitivity of surface wave phase delays to fractional perturbations in $1/Q$ (Zhou 2009). To estimate the effects of a low-Q lithosphere, we generate synthetic seismograms in our reference 1-D Q model with/without the top 80 km layer replaced by a constant Q of 300 and compare surface wave traveltimes. At an epicentral distance of 150 degree, 50-s Love waves are delayed by 5 s, 100- and 200-s Love waves are delayed by 3 s, Rayleigh
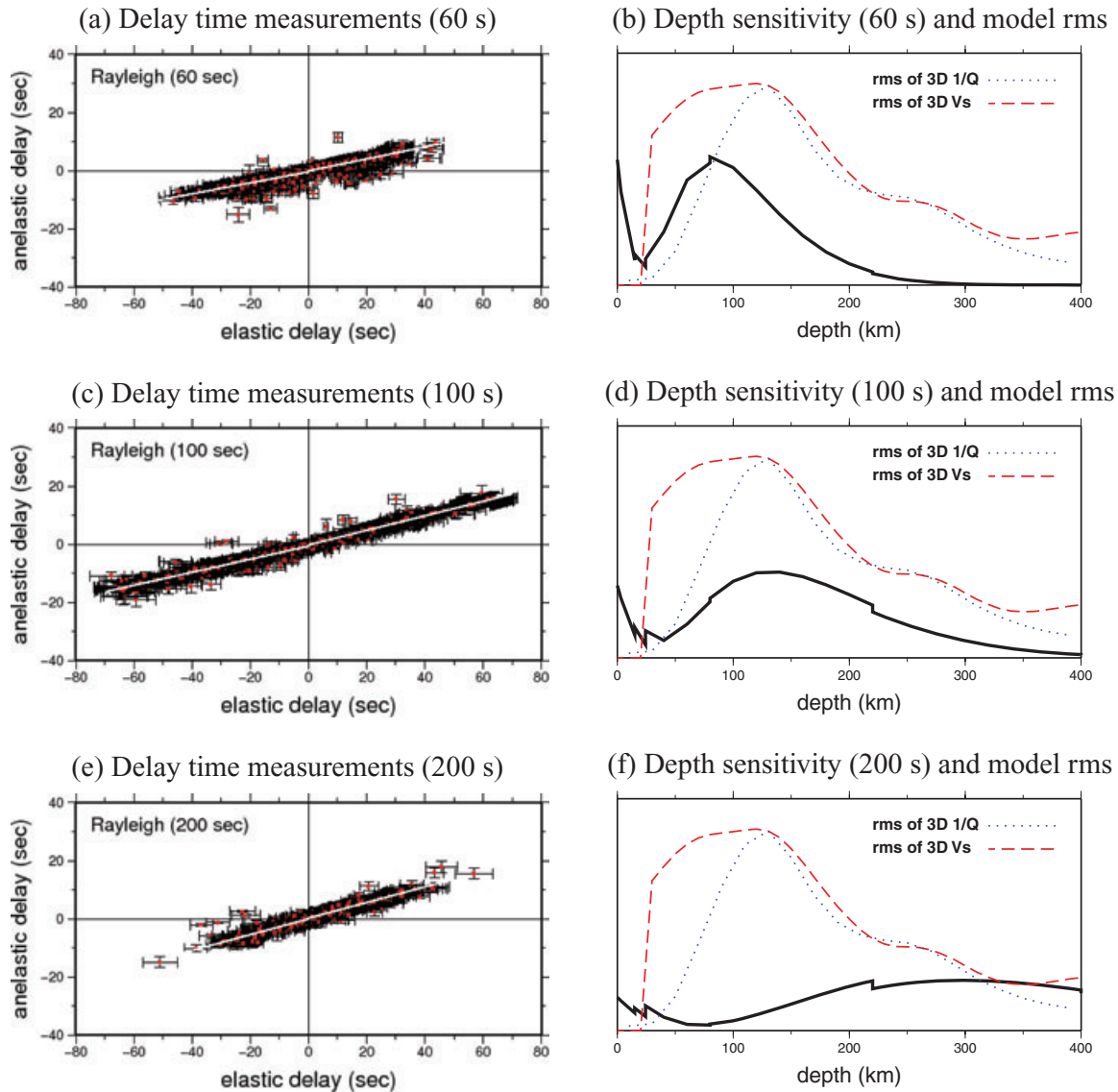
Anelastic effects on Rayleigh-wave phase delays

(a) Delay time measurements (60 s)

(b) Depth sensitivity (60 s) and model rms

(c) Delay time measurements (100 s)

(d) Depth sensitivity (100 s) and model rms

(e) Delay time measurements (200 s)

(f) Depth sensitivity (200 s) and model rms

Figure 7. The same as Fig. 6 but for Rayleigh waves. Strong frequency dependence of anelastic effects is also observed in Rayleigh-wave phase delays. The fitted ratios of anelastic delays to elastic delays are 0.21 at 60 s, 0.24 at 100 s and 0.27 at 200 s. 3-D anelastic effects on Rayleigh waves are systematically more significant than Love waves because Rayleigh waves are more sensitive to structures in the low Q zone (80–300 km) in our model.

waves at all periods are delayed by less than 2 s. Considering uncertainties in our measurements, the effects of a low Q value in the top 80 km are negligible in long-period Love waves and Rayleigh waves. For short-period Love waves, lower Q values in the top 80 km can lead to slightly stronger 3-D anelastic dispersion than seen in Fig. 6.

It is important to point out that while anelastic delays and elastic delays are highly correlated, their relation is not linear. Moreover, due to 3-D wave propagation effects, elastic advances in surface wave traveltimes are not necessarily always associated with anelastic advances, sometimes they are accompanied with no advance or even weak anelastic delays. For waves propagating through dominantly fast anomalies, large elastic traveltime advances (negative delays) are observed, the anelastic advances do not increase linearly with elastic advances but show a weak flattening pattern in the scatterplot. The weakening of anelastic effects in seismically

fast ('cold') regions becomes more apparent for purely continental paths, and the path dependence will be discussed in more detail in Section 6.

It is worth noting that (1) the fact 15–20 per cent of observed phase delays can be attributed to 3-D Q structure does not necessarily indicate current velocity tomographic models (e.g. S20RTS) have been overestimated. This is because inaccuracy in tomographic theory will introduce internal inconsistency in the inverse system, which often requires greater damping to be applied in the inversion; (2) the relative contribution of 3-D elastic and 3-D anelastic effects in surface wave phase delays does not depend on the rms of the 'elastic' wave speed model (S20RTS) used in this paper; and (3) we have assumed a thermal origin of mantle wave speed and Q anomalies, other effects such as water content and partial melting can also be important but they have not been well constrained in mineral physics and are beyond the scope of this study.

5 THE EFFECTS OF MINERALOGICAL PARAMETERS

In this section, we examine the dependence of 3-D anelastic effects on mineralogical parameters that control both the 1-D reference Q model and the conversion from 3-D velocity model to 3-D Q model. We experiment with additional two sets of rheology parameters to investigate the effects of rheology parameters on the resulting Q models. The rheology parameters are listed in Table 2 and the corresponding 1-D Q models are labeled as $\mathbf{Q1DM_L}$, $\mathbf{Q1DM_M}$ and $\mathbf{Q1DM_H}$, where model $\mathbf{Q1DM_M}$ is the 1-D Q model we used in Sections 3 and 4 and it is comparable to PREM (Figs 1 and 8). In generating model $\mathbf{Q1DM_L}$ we used a slightly smaller activation energy $E^* = 420\,\mathrm{KJ\,mol^{-1}}$ and a relatively higher activation volume $V^* = 19\,\mathrm{cm^3\,mol^{-1}}$; and for model $\mathbf{Q1DM_H}$ we used a larger activation energy $E^* = 520\,\mathrm{KJ\,mol^{-1}}$ and a smaller activation volume $V^* = 15\,\mathrm{cm^3\,mol^{-1}}$. We adjust the mineralogical parameters accordingly such that the overall Q values in the mantle are smaller than PREM in model $\mathbf{Q1DM_L}$ and larger than PREM in model $\mathbf{Q1DM_H}$. (Fig. 8). The corresponding 3-D Q models, $\mathbf{Q3DM_L}$ and $\mathbf{Q3DM_H}$, are calculated from 3-D velocity model S20RTS for the additional two sets of mineralogical parameters ($\mathbf{M_L}$ and $\mathbf{M_H}$) using the same algorithm that has been discussed in Section 3.2. Maps of the 3-D Q models at a depth of 100 km are plotted in Fig. 9. We ran

Table 2. Rheology parameters for different anelasticity (Q) models.

Parameter set	E^* (KJ mol^{-1})	V^* (cm^3 mol^{-1})	A
$\mathbf{M_L}$	420	19	1.394
$\mathbf{M_M}$	470	17	1.394
$\mathbf{M_H}$	520	15	1.394

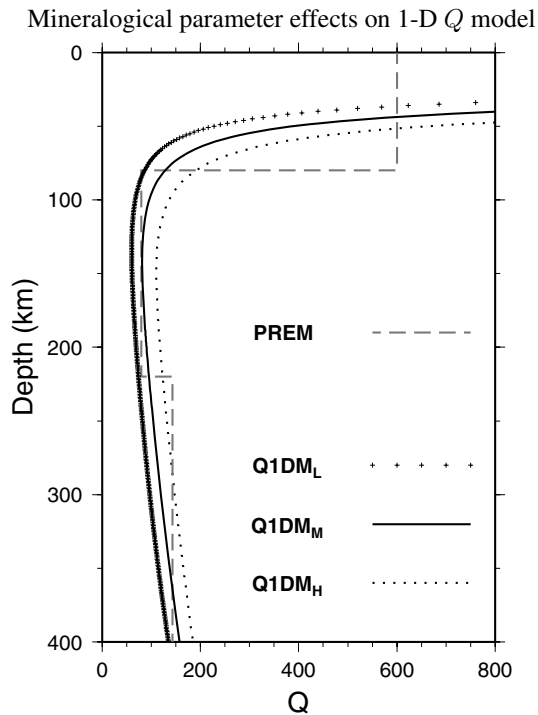### Mineralogical parameter effects on 1-D Q model

Figure 8. Reference Q models constructed using three different mineralogical parameter sets (see Table. 2). Q values in $\mathbf{Q1DM_M}$ are moderate and comparable to PREM at depths between 80 and 220 km, Q values are higher than PREM in model $\mathbf{Q1DM_H}$ and lower than PREM in model $\mathbf{Q1DM_L}$. PREM Q model is plotted in grey dashed line for reference.

wave propagation experiments in the two additional sets of global Q models, and make phase delay measurements following the same procedure as described in Section 3.3.

Our measurements show that the effects of 3-D anelastic dispersion are dependent upon mineralogical parameters used in the experiment. Scatterplots of 100-s Rayleigh-wave phase delays are plotted in Fig. 9. The ratio of anelastic phase delays to elastic phase delays depends upon mineralogical parameters: measurements made for 3-D Q model $\mathbf{Q3DM_L}$ show that the slope of the scatterplot is roughly 0.28, and the ratio decreases to ~0.24 in Q model $\mathbf{Q3DM_M}$ and it deceases further to ~0.21 for model $\mathbf{Q3DM_H}$.

Least square fitted ratios of anelastic to elastic delay times for Love waves and Rayleigh waves for the three sets of global Q models are shown in Fig. 9. The elastic delays are identical in the three groups, while anelastic delays vary with mineralogical parameters applied in generating the 1-D and 3-D Q models. The grey bars are ratios at periods ranging from 60 to 200 s. The frequency dependence of anelastic dispersion shows a similar pattern in the three experiments: anelastic dispersion is more significant at longer periods, and the frequency dependence is most apparent in the period range between 60 and 150 s and becomes weaker at longer periods (150–200 s), especially for Rayleigh waves.

In the case of using the mineralogical parameter set $\mathbf{M_L}$, the anelastic dispersion effects on surface wave phase delays are the largest at all periods for both Love waves and Rayleigh waves in spite of the smallest fractional perturbations in $1/Q$ among the three 3-D Q models (Fig. 9). It is worth emphasizing that (1) both the reference Q models and perturbations in Q are calculated from mantle temperature using three different sets of mineralogical parameters; (2) anelastic delay times are introduced by perturbations in Q, while temperature partial derivatives are dependent also upon the reference Q values, and overall the 3-D anelastic dispersion effects become stronger when the mineralogical parameters used are associated with lower reference Q values and (3) we shall keep in mind that uncertainties in mineralogical parameters will lead to uncertainties in 3-D anelastic dispersion effects as illustrated in Fig. 9.

6 PATH DEPENDENCE OF 3-D ANELASTIC EFFECTS

Our measurements show that 3-D anelastic effects on surface wave phase delays are path dependent. We select measurements with their great-circle ray paths mainly travelling through oceanic regions as well as those with their great-circle paths mainly in continental regions. Phase-delay measurements for 100-s Love waves and Rayleigh waves and associated ray paths are plotted in Figs 10 and 11 for comparison of oceanic paths and continental paths.

In the upper mantle, there is strong correlation between velocity model S20RTS and tectonic features. The oceanic regions are underlain by slower ('hotter') mantle material while stable continents are associated with faster ('colder') lithosphere and mantle. As expected, the scatterplot of elastic-anelastic phase delays for oceanic paths is dominated by positive traveltime delays and measurements of continental paths are dominated by negative traveltime delays. In Fig. 10, the ratio of anelastic delays to elastic phase delays of 100 s Love waves is close to 0.2 for oceanic paths. For continental paths, there is apparent 'flattening' on the scatterplot: waves travelling through 'colder' regions experience larger phase advances but not significant increase in 3-D anelastic dispersion. The 'flattening' is unlikely due to Love-wave higher-mode contamination because (1) we have excluded records contaminated by higher modes from our measurements; (2) higher modes would affect both the elastic and
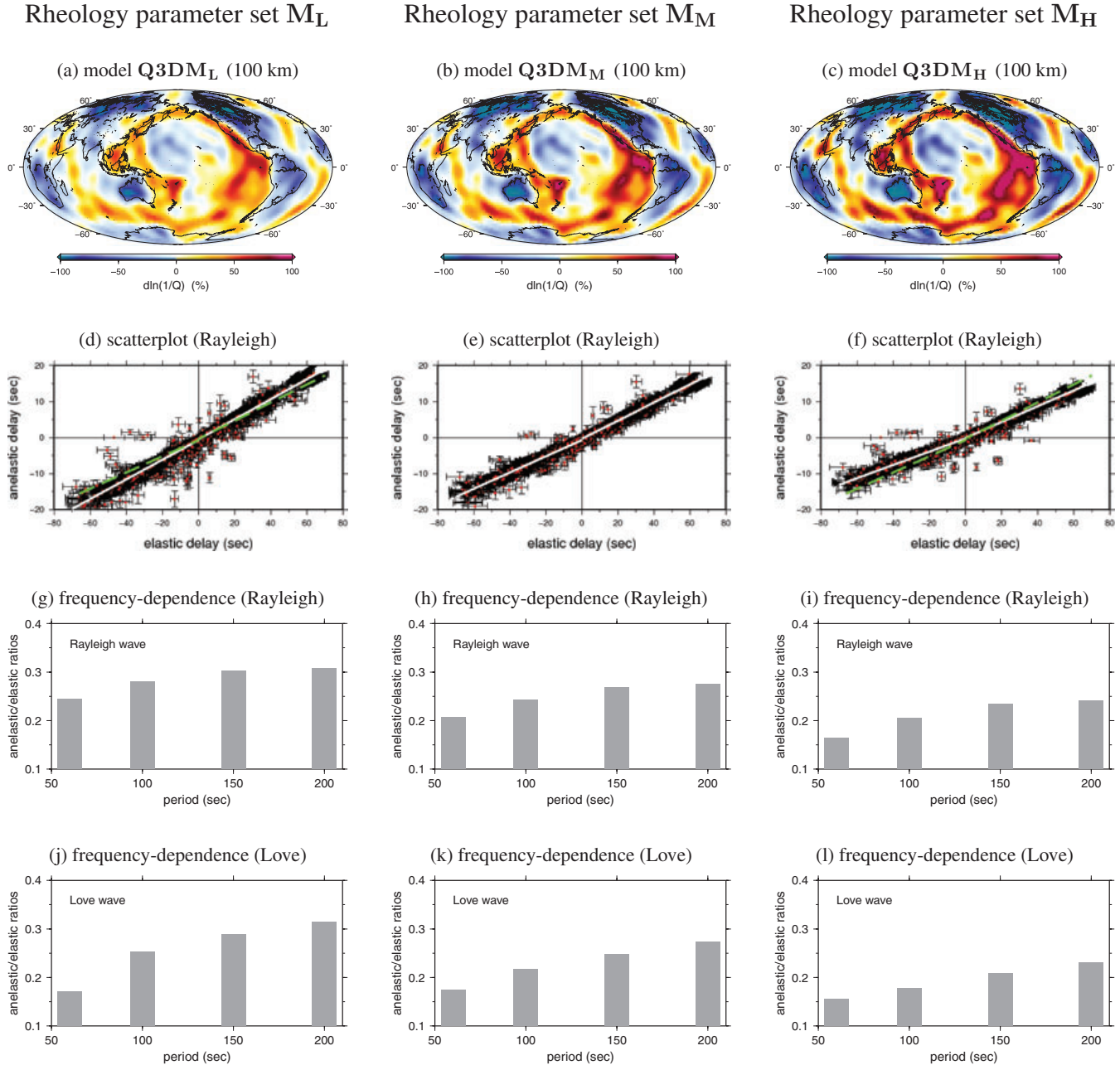
Mineralogical parameter effects on 3-D Q model and anelastic phase delays

Rheology parameter set $\mathbf{M_L}$ Rheology parameter set $\mathbf{M_M}$ Rheology parameter set $\mathbf{M_H}$

(a) model $\mathbf{Q3DM_L}$ (100 km)   (b) model $\mathbf{Q3DM_M}$ (100 km)   (c) model $\mathbf{Q3DM_H}$ (100 km)

(d) scatterplot (Rayleigh)   (e) scatterplot (Rayleigh)   (f) scatterplot (Rayleigh)

(g) frequency-dependence (Rayleigh)   (h) frequency-dependence (Rayleigh)   (i) frequency-dependence (Rayleigh)

(j) frequency-dependence (Love)   (k) frequency-dependence (Love)   (l) frequency-dependence (Love)

Figure 9. Delay-time measurements for three sets of global Q models generated using mineralogical parameters $\mathbf{M_L}$, $\mathbf{M_M}$ and $\mathbf{M_H}$; (a), (b) and (c) are maps of fractional perturbations in $1/Q$ ($\delta\ln Q^{-1}$) at a depth of 100 km, and corresponding reference (1-D) Q models are plotted in Fig. 8; (d), (e) and (f) are scatterplots of elastic delays versus anelastic delays for 100-s Rayleigh waves, the ratio of anelastic delay to elastic delay decreases from ∼0.28 (parameter set $\mathbf{M_L}$) to ∼0.21 (parameter set $\mathbf{M_H}$). The best fitting line in (e) is also plotted as green dashed lines in (d) and (f) for comparison. (g), (h), and (i) are the ratios (grey bars) of anelastic delay to elastic delay of Rayleigh waves at periods of 60, 100, 150 and 200 s. These ratios come from least-square fitting of measurements. The 3-D anelastic effects are frequency-dependent and the frequency dependence is most apparent in the period range between 60 and 150 s. Note fractional perturbations in $1/Q$ are the smallest in model $\mathbf{Q3DM_L}$, while the associated anelastic delay times are largest due to the associated low Q values in the reference model $\mathbf{Q1DM_L}$ (Fig. 8).

anelastic measurements and therefore will not result in 'flattening' in anelastic measurements and (3) the 'flattening' is expected based upon the non-linear relation between 'elastic' and 'anelastic' delays which will be discussed in Section 7.

We calculate global phase-velocity maps of 100-s Love waves in the four models listed in Table 1. The differences in phase ve-

locities between model (I) and (II) are due to 3-D elastic structure ($c_{3-\mathrm{DV}} - c_{1-\mathrm{DV}}$), and they are plotted in Fig. 10(e). The fractional perturbations $\delta c/c$ with respect to $c_{1-\mathrm{DV}}$ are in the range of -4.1–4.7 per cent. The differences in phase velocities between model (III) and (IV) are due to 3-D anelastic structure ($c_{3-\mathrm{DQ}} - c_{1-\mathrm{DQ}}$) and the perturbations with respect to $c_{1-\mathrm{DQ}}$ are plotted

(a) Oceanic paths

(b) Continental paths

(c) Love-wave scatterplot (oceanic)

(d) Love-wave scatterplot (continental)

(e) Phase velocity map ($c_{3D\ V} - c_{1D\ V}$)

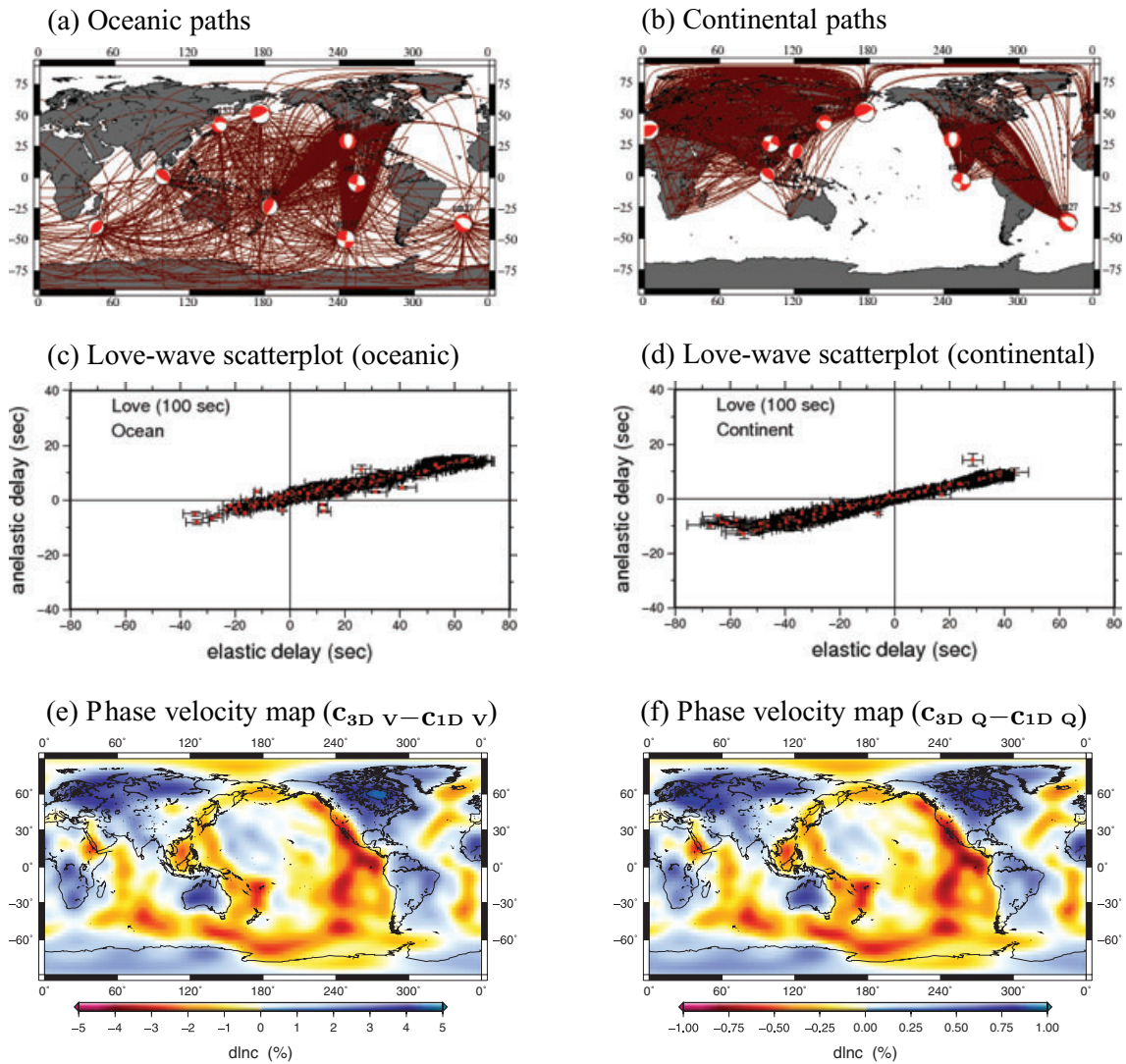## (f) Phase velocity map ($c_{3D\ Q} - c_{1D\ Q}$)

Figure 10. Path dependence of anelastic effects on Love-wave phase delays. Top: (a) and (b) are map views of oceanic paths (1502 paths) and continental paths (2665 paths), respectively. Love-wave delay-time scatterplots for the two groups of paths are plotted in (c) and (d), respectively. The continental scatterplot shows some 'flattening' indicating that anelastic effects are weaker for continental paths than for oceanic paths. (e) and (f) are phase velocity maps of 100-s Love waves corresponding to 3-D velocity and 3-D Q structure, respectively. Fractional perturbations in phase velocity ($\delta \ln c$) varies from -4.1 per cent to 4.7 per cent in (e) and from -0.89 per cent to 0.86 per cent in (f). Note different colour scales have been used in (e) and (f).

in Fig. 10(f), and the perturbations are in the range of -0.89 to 0.86 per cent. The amplitude of the fractional perturbations in local phase velocities due to 3-D velocity structure is about three to four times stronger than that due to 3-D anelastic structure (note the different colour scales in Fig. 10). The ratio between local $\delta c/c$ caused by 3-D velocity structure and those caused by 3-D Q structure are location dependent, and, they are generally smaller in continental areas than in oceanic areas.

In Fig. 11, we compare measurements made for oceanic paths and continental paths for 100-s Rayleigh waves. Rayleigh wave phase-delay measurements for oceanic paths are dominated by traveltime delays (slow anomalies), and the ratio of anelastic delays to elastic phase delays is close to 0.25, and it is larger than the ratio for Love waves at the same period. For continental paths, the flattening of the scatterplot is not as apparent as 100-s Love waves, and the ratio is close to 0.24. Overall, 3-D anelastic dispersion effects on phase delays are slightly stronger in oceanic paths than in continen-

tal paths. We calculate maps of 100-s Rayleigh-wave phase velocity perturbations due to 3-D Q structure ($c_{3-DQ} - c_{1-DQ}$), and the fractional perturbations are in the range of -0.79–0.85 per cent while the perturbations due to 3-D elastic structure ($c_{3-DV} - c_{1-DV}$) vary from -3.5 to 3.9 per cent, relatively weaker than those for 100-s Love waves. As a result, 3-D Q structures have more significant effects on Rayleigh waves than on Love waves—this is consistent with the slope variations in the measurement scatterplots.

We conclude that (1) the effects of 3-D anelasticity on phase delays are more significant in oceanic paths than in continental paths, that is, the effects of 3-D anelastic dispersion on phase advances are less significant than that on phase delays. This is mainly due to the non-linear relation between 'elastic' and 'anelastic' velocity perturbations in the case of a common thermal origin and (2) the path dependence is more apparent for Love waves than for Rayleigh waves. In Section 7, we verify the non-linear relation for local S waves using a simple analytical approach.

(a) oceanic paths

(b) continental paths

(c) Rayleigh-wave scatterplot (oceanic)

(d) Rayleigh-wave scatterplot (continental)

(e) phase velocity map ($\mathbf{c}_{3D\ V} - \mathbf{c}_{1D\ V}$)

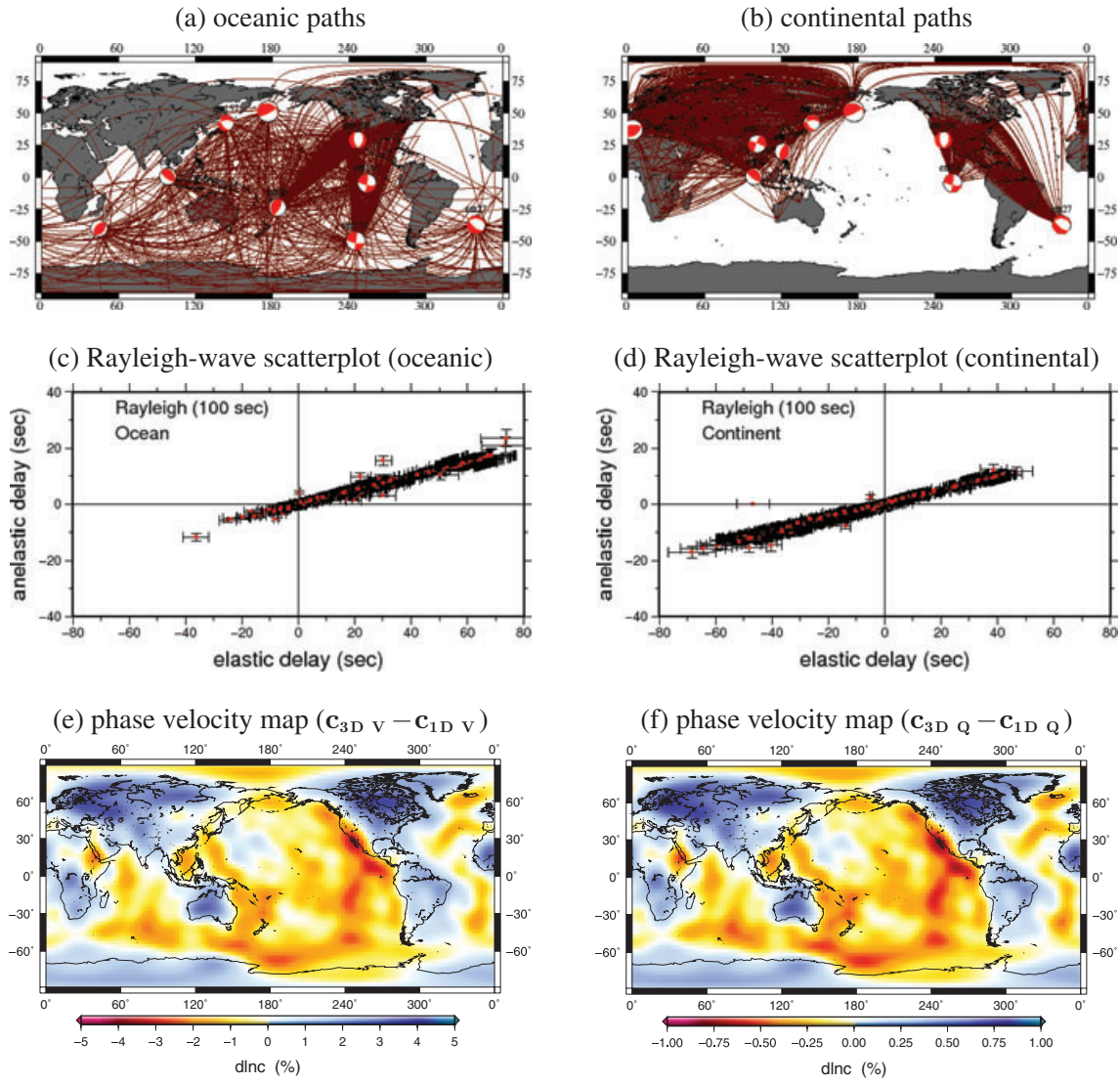(f) phase velocity map ($\mathbf{c}_{3D\ Q} - \mathbf{c}_{1D\ Q}$)

Figure 11. The same as Fig. 10 but for Rayleigh waves, there are 1,499 oceanic paths and 2578 continental paths. The slope of the scatterplots is 0.25 for oceanic paths and is 0.24 for continental paths. (e) and (f) are phase-velocity maps of 100-s Rayleigh waves corresponding to 3-D velocity and 3-D Q structure, respectively. Fractional variations in phase velocity range from −3.5 per cent to 3.9 per cent in (e) and −0.79 per cent to 0.82 per cent in (f). Note different colour scales have been used in (e) and (f).

7 ANALYTICAL VERIFICATIONS

Surface waves are mainly constructive interactions of multiple reflected S waves. To the first order for small perturbations in Q in eq. (3), local perturbations in S-wave velocity due to local perturbations in $Q \rightarrow Q + \delta Q$ can be written as

$$\left(\frac{\delta V_S}{V_S}\right)_{3-DQ} = -\frac{1}{Q\pi} \ln\left(\frac{\omega}{\omega_0}\right) \frac{\delta Q}{Q}, \tag{10}$$

where $Q = Q_\mu$ is the local quality factor for shear modulus. Assuming local Q perturbations are due to temperature perturbations, $\delta Q/Q$ can be related to perturbations in temperature δT in eq. (9), yielding

$$\left(\frac{\delta V_S}{V_S}\right)_{3-DQ} = \frac{\alpha}{Q\pi} \ln\left(\frac{\omega}{\omega_0}\right) \frac{E^* + PV^*}{RT^2} \delta T. \tag{11}$$

The temperature partial derivative in eq. (8) can be used to find the associated velocity perturbations at the reference Q value,

$$\left(\frac{\delta V_S}{V_S}\right)_{3-DQ} = \frac{\alpha}{Q\pi} \ln\left(\frac{\omega}{\omega_0}\right) \frac{E^* + PV^*}{RT^2} \left(\frac{\partial \ln V_S}{\partial T}\right)^{-1}$$
$$\times \left(\frac{\delta V_S}{V_S}\right)_{3-DV}. \tag{12}$$

To the first order assuming thermal anomalies, fractional perturbations in anelastic dispersion introduced by local variations in anelasticity $(\delta V_S/V_S)_{3-DQ}$ are related to fractional perturbations in S-wave velocity $(\delta V_S/V_S)_{3-DV}$ at the reference Q. This relation is not linear but dependent upon the background Q value as well as temperature T. In Fig. 12, we calculate local 3-D anelastic dispersions $(\delta V_S/V_S)_{3-DQ}$ associated with velocity variations $(\delta V_S/V_S)_{3-DV}$ in the range of −3 to 3 per cent for reference Q and temperature values at depths of 100, 150, 200, 300 and 400 km. We use an iterative approach and update temperature, Q and the partial derivative $\partial \ln V_S/\partial T$ in the calculations of $(\delta V_S/V_S)_{3-DQ}$
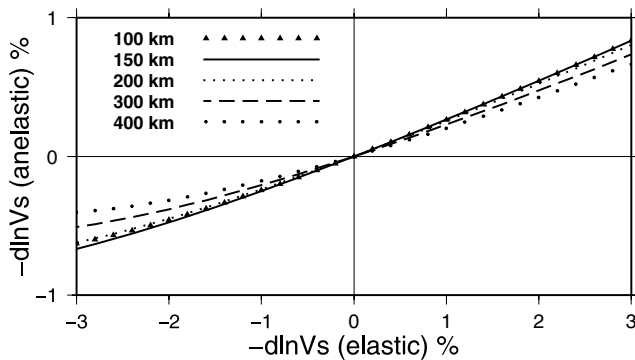
Figure 12. Predicted elastic velocity perturbations versus anelastic velocity perturbations for 100-s shear waves calculated using eq. (12) at different depths using an iterative approach. The relation between elastic and anelastic velocity perturbations is not linear and the ratio between anelastic and elastic velocity perturbations becomes larger for 'hot' anomalies. For example, at a depth of 100 km, 2 per cent 'elastic' velocity reduction is associated with 0.54 per cent 'anelastic' velocity reduction, while 2 per cent 'elastic' velocity increase is associated with 0.46 per cent 'anelastic' velocity increase. The ratio between anelastic and elastic velocity perturbations also depends upon the background Q value, for example, the ratio increases from 0.22 at 400 km (reference $Q = 157.6$) to 0.28 at 150 km (reference $Q = 81.7$). Note that these calculations are for local perturbations in velocity and Q, and can not be directly compared with phase-delay measurements as surface wave delays are integrated effects of local perturbations over depth as well as over the ray path.

until eq. (12) converges. The mineralogical parameters as well as the reference thermal structure have been described in Section 3.1.

The relation between local perturbations in $(\delta V_S / V_S)_{3-DQ}$ and $(\delta V_S / V_S)_{3-DV}$ in Fig. 12 is generally consistent with our surface wave phase delay measurements—the ratio between $(\delta V_S / V_S)_{3-DQ}$ and $(\delta V_S / V_S)_{3-DV}$ is roughly between 0.13 and 0.28. The curves flatten out for large negative perturbations in $-(\delta V_S / V_S)_{3-DV}$, indicating that the effects of 3-D anelastic dispersion in fast (cold) regions are not as significant as in slow (hot) regions for the same amount of absolute perturbations in local $(\delta V_S / V_S)_{3-DV}$. For example, when temperature increases, 1 per cent 'elastic' S-wave velocity reduction at a depth of 100 km is associated with 0.26 per cent 'anelastic' velocity reduction, while 2 per cent 'elastic' velocity reduction is associated with 0.54 per cent 'anelastic' velocity reduction. In the case of temperature decrease, 1 per cent 'elastic' velocity increase is associated with 0.24 per cent 'anelastic' velocity increase, and 2 per cent 'elastic' velocity increase is associated with 0.46 per cent 'anelastic' velocity increase. This is consistent with the 'flattening' of anelastic phase advances observed for the continental paths as described in Section 6.

It is important to point out this analysis is based purely upon local perturbations in Q and velocity. The curves in Fig. 12 cannot be directly compared with phase delay measurements as surface wave phase delays are integrated effects of local perturbations over depth as well as over the ray path. For example, large surface wave phase delays in 3-D velocity models do not necessary correspond to large local velocity perturbations but may be a result of surface waves propagating though large provinces of weak anomalies.

8 CONCLUSION

We investigate the effects of lateral variations in anelasticity (Q) on long-period surface wave phase delays by simulating wave propagation in earth models with 3-D wave speed structures and 3-

D Q structures using the Spectral Element Method (Komatitsch & Tromp 1999, 2002). We compare phase delays caused by 3-D Q structure with phase delays caused by 3-D wave speed structure and conclude that 3-D Q structures in the mantle have significant effects on long-period surface wave phase delays. At a period of 100 s, the ratio between phase delays caused by 3-D Q structure and those caused by 3-D velocity structure is roughly between 0.21 and 0.24, indicating that roughly 15–20 per cent of observed phase delays are due to 3-D Q structure. These effects have so far been ignored in present-day tomographic studies and may have led to biased tomographic structures. The coupling between elastic and anelastic effects in surface wave traveltimes indicates that a joint inversion of 3-D velocity and 3-D Q structure using both traveltimes and amplitudes is necessary. The resulting self-consistent 3-D velocity and 3-D Q models will be very helpful in mapping lateral thermal and compositional heterogeneities in the upper mantle.

Our numerical experiments show that 3-D anelastic dispersion effects on surface wave phase delays depend upon the frequency of the waves due to local S-wave anelastic dispersion, frequency-dependent depth sensitivity of surface waves as well as the 3-D distribution of Q anomalies. The 3-D anelastic effects generally increase with increasing wave period and the frequency dependence is most apparent in the period range between 60 and 150 s in our numerical experiments as Q variations are the strongest in the asthenosphere.

In a thermal model, the significance of the 3-D anelastic dispersion effects depend upon mineralogy parameters, that is, activation energy and activation volume. The 3-D Q model used in this paper is constructed using the 3-D wave speed model S20RTS assuming that both velocity and Q perturbations are due to temperature variations. Delay times introduced by the 3-D velocity structure and those introduced by the corresponding 3-D Q structure are therefore correlated, but the correlation is not linear: the ratio between anelastic and elastic delays (or advances) becomes larger for 'hotter' anomalies than for 'colder' anomalies.

REFERENCES

Anderson, D.L. & Minster, J.B., 1979. The frequency dependence of Q in the Earth and implications for mantle rheology and Chandler wobble, *Geophys. J. Int.,* **58,** 431–440.

Béjina, F., Jaoul, O. & Liebermann, R.C., 2003. Diffusion in minerals at high pressure: a review, *Phys. Earth planet. Inter.,* **139,** 3–20.

Billien, M., Lèvêque, J.-J. & Trampert, J., 2000. Global maps of Rayleigh wave attenuation for periods between 40 and 150 seconds, *Geophys. Res. Lett.,* **27,** 3619–3622.

Dalton, C. & Ekström, G., 2006. Global models of surface wave attenuation, *J. geophys. Res.,* **111,** B05317, doi:10.1029/2005JB003997.

Dalton, C., Ekström, G. & Dziewoński, A.M., 2008. The global attenuation structure of the upper mantle, *J. geophys. Res.,* **113,** B09303, doi:10.1029/2007JB005429.

Dahlen, F.A. & Tromp, J., 1998. *Theoretical Global Seismology,* Princeton University Press, Princeton, New Jersey.

Duffy, T.S. & Anderson, D.L., 1989. Seismic velocities in mantle minerals and the mineralogy of the upper mantle, *J. geophys. Res.,* **94,** 1895–1912.

Durek, J.J. & Ekström, G., 1996. A radial model of anelasticity constraint with long-period surface wave attenuation, *Bull. seism. Soc. Am.,* **86,** 144–158.

Dziewonski, A.M. & Anderson, D.L., 1981. Preliminary reference Earth Model, *Phys. Earth planet. Inter.,* **25,** 297–356.

Faul, U.H. & Jackson, I., 2005. The seismological signature of temperature and grain size variations in the upper mantle, *Earth planet. Sci. Lett.,* **234,** 119–134.

Grand, S.P., 1987. Tomographic inversion for shear velocity beneath the North American plate. *J. geophys. Res.,* **92,** 14 065–14 090.

Gung, Y. & Romanowicz, B., 2004. Q tomography of the upper mantle using three-component long-period waveforms, *Geophys. J. Int.,* **157,** 813–830.

Isaak, D.G., 1992. High-temperature elasticity of iron-bearing olivines, *J. geophys. Res.,* **97,** 1871–1885.

Jackson, I., 2000. Laboratory Measurements of Seismic Wave dispersion and Attenuation: Recent Progress., in *Earth's Deep Interior: Mineral Physics and Tomography from the Atomic to the Global Scale,* Vol. 117, pp. 265–289, eds Karato, S., Forte, R., Liebermann, G., Masters, G. & Stixrude, L., American Geophysical Union, Washington, DC.

Jackson, D.D. & Anderson, D.L., 1970. Physical mechanisms of seismic-wave attenuation, *Rev. Geophys.,* **8**(1), 1–63.

Jackson, I. & Paterson, M.S., 1993. A high-pressure, high-temperature apparatus for studies of seismic wave dispersion and attenuation, *Pure appl. Geophys.,* **141,** 445–466.

Jackson, I., Fitz Gerald, J.D., Faul, U.H. & Tan, B.H., 2002. Grain-size sensitivity seismic wave attenuation in polycrystalline olivine, *J. geophys. Res.,* **107,** B122360, doi:10.1029/2001JB001225.

Kanamori, H. & Anderson, D.L., 1977. Importance of physical dispersion in surface-wave and free-oscillation problems—review, *Rev. Geophys. Space Phys.,* **15,** 105–112.

Karato, S.-I., 1993. Importance of anelastic in the interpretation of seismic tomography, *Geophys. Res. Lett.,* **20**(15), 1623–1626.

Karato, S. & Spetzler, H.A., 1990. Defect microdynamics in mineral and solid-state mechanisms of seismic wave attenuation and velocity dispersion in the mantle, *Rev. Geophys.,* **28,** 399–421.

Komatitsch, D. & Tromp, J., 1999. Introduction to the spectral-element method for 3-D seismic wave propagation, *Geophys. J. Int.,* **139,** 806–822.

Komatitsch, D. & Tromp, J., 2002. Spectral-element simulations of global seismic wave propagation—I. Validation, *Geophys. J. Int.,* **149,** 390–412.

Laske, G. & Master, G., 1996. Constraints on global phase velocity maps from long-period polarization data, *J. geophys. Res.,* **101**(B7), 16 059–16 075.

Liu, H.P., Anderson, D.L. & Kanamori, H., 1976. Velocity dispersion due to anelasticity; implications for seismology and mantle composition, *Geophys. J. R. astr. Soc.,* **47,** 41–58.

Master, G., Johnson, S., Laske, G. & Bolton, H., 1996. A shear-velocity model of the mantle, *Phil. Trans. R. Soc. Lond., A,* **354,** 1385–1411.

Reid, F.J.L., Woodhouse, J.H. & Van Heijst, H.J., 2001. Upper mantle attenuation and velocity structure from measurements of differential *S* phases, *Geophys. J. Int.,* **145,** 615–630.

Ritsema, J. & Van Heijst, H.J., 2000. Seismic imaging of structural heterogeneity in Earth's mantle: evidence for large-scale mantle flow, *Sci. Prog.,* **83,** 243–259.

Romanowicz, B., 1995. A global tomographic model of shear attenuation in the upper mantle, *J. geophys. Res.,* **100,** 12 375–12 394.

Selby, N.D. & Woodhouse, J.H., 2000. Controls on Rayleigh wave amplitudes: attenuation and focusing, *Geophys. J. Int.,* **142,** 933–940.

Selby, N.D. & Woodhouse, J.H., 2002. The Q structure of the upper mantle: constraints from Rayleigh wave amplitudes, *J. geophys. Res.,* **107**(B5), 2097, doi:10.1029/2001JB000257.

Shapiro, N.M. & Ritzwoller, M.H., 2004. Thermodynamic constraints on seismic inversions, *Geophys. J. Int.,* **157,** 1175–1188.

Shito, A., Karato, S. & Park, J., 2004. Frequency dependence of Q in Earth's upper mantle inferred from continuous spectra of body waves, *Geophys. Res. Lett.,* **31,** L12603, doi:10.1029/2004GL019582.

Slepian, D., 1978. Prolate spheroidal wave functions, Fourier analysis and uncertainty, V: the discrete case, *Bell Syst. Tech. J.,* **57,** 1371–1429.

Smith, M.L. & Dahlen, F.A., 1981. The period and Q of the Chandler wobble, *Geophys. J. Int.,* **64,** 223–281.

Su, W.-J., Woodward, R.L. & Dziewonski, A.M., 1994. Degree 12 model of shear velocity heterogeneity in the mantle. *J. geophys. Res.,* **99,** 6945–6980.

Warren, L.M. & Shearer, P.M., 2002. Mapping lateral variations in upper mantle attenuation by stacking *P* and *PP* spectra, *J. geophys. Res.,* **107,** B122342, doi:10.1029/2001JB001195.

Wessel, P. & Smith, W.H.F., 1995. New Version of the Generic Mapping Tools Released, *EOS, Trans. Am. geophys. Un.,* **76,** 329.

Zhou, Y., 2009. Surface-wave sensitivity to 3-D anelasticity, *Geophys. J. Int.,* **178,** 1403–1410.

Zhou, Y., Dahlen, F.A. & Nolet, G., 2004. Three-dimensional sensitivity kernels for surface wave observables, *Geophys. J. Int.,* **158,** 142–168.

Zhou, Y., Nolet, G., Dahlen, F.A. & Laske, G., 2006. Global upper-mantle structure from finite-frequency surface-wave tomography, *J. geophys. Res.,* **111,** B04304, doi:10.1029/2005JB003677.